

A Search for Vulcanoids with the STEREO Heliospheric Imager

A. J. Steffl¹, N. J. Cunningham², A. B. Shinn¹, D. D. Durda¹, and S. A. Stern³

ABSTRACT

Interior to the orbit of Mercury, between 0.07 and 0.21 AU, is a dynamically stable region where a population of asteroids, known as Vulcanoids, may reside. We present the results from our search for Vulcanoids using archival data from the Heliospheric Imager-1 (HI-1) instrument on NASA's two STEREO spacecraft. Four separate observers independently searched through images obtained from 2008-12-10 to 2009-02-28. Roughly, all Vulcanoids with $e \leq 0.15$ and $i \leq 15^\circ$ will pass through the HI-1 field of view at least twice during this period. No Vulcanoids were detected. Based on the number of synthetic Vulcanoids added to the data that were detected, we derive a 3σ upper limit (i.e. a confidence level > 0.997) that there are presently no Vulcanoids larger than 5.7 km in diameter, assuming an R-band albedo of $p_R=0.05$ and a Mercury-like phase function. The present-day Vulcanoid population, if it exists at all, is likely a small remnant of the hypothetical primordial Vulcanoid population due to the combined effects of collisional evolution and subsequent radiative transport of collisional fragments. If we assume an extant Vulcanoid population with a collisional equilibrium differential size distribution with a power law index of -3.5, our limit implies that there are no more than 76 Vulcanoids larger than 1 km.

Subject headings: Asteroids, Mercury, Image processing

1. Introduction

¹ Interior to Mercury's orbit is a dynamically stable region where a population of small,
² asteroid-like bodies called Vulcanoids has long been hypothesized to exist, cf. review by

¹Department of Space Studies, Southwest Research Institute, Boulder, CO 80302

²Department of Physics, Nebraska Wesleyan University, Lincoln, NE 68504

³Space Science and Engineering Division, Southwest Research Institute, Boulder, CO 80302

3 Campins et al. (1996). This region, known as the Vulcanoid zone, extends from roughly 0.07
4 AU to 0.21 AU (15–45 solar radii). Seen from Earth, objects in the Vulcanoid zone have
5 maximum solar elongation angles of just 4–12°. The outer boundary of the Vulcanoid zone,
6 at 0.21 AU, is set by dynamical instability. Objects with semi-major axes greater than this
7 limit evolve onto Mercury-crossing orbits on 100-Myr timescales due to orbital perturbations
8 caused by both Mercury and Venus (Evans and Tabachnik 1999, 2002). The inner edge of
9 the Vulcanoid zone is less well-defined, but is set by the combination of the intense thermal
10 environment and dynamical transport mechanisms such as Poynting-Robertson drag and
11 the Yarkovsky effect. At 0.06 AU (13 solar radii) solar radiation is so intense that even
12 a pure iron body 100 km in diameter will evaporate in less than 4.5 Gyr (Lebofsky 1975;
13 Campins et al. 1996). The time an object can survive against evaporation is a strong function
14 of heliocentric distance, such that, at 0.07 AU, a pure iron body of just 2 km diameter
15 will survive for the current age of the solar system. Poynting-Robertson drag extends the
16 evaporation limit outward, as it can move a 2-km diameter object with $\rho = 4 \text{ g cm}^{-3}$ from
17 0.08 to 0.07 AU in 4 Gyr, where it will evaporate (Stern and Durda 2000).

18 The detection of one or more members of the putative Vulcanoid population is of interest
19 as it would represent the discovery of a whole new class of solar system objects. If they existed
20 at all, primordial Vulcanoids likely formed from the highest temperature condensates near the
21 inner edge of the solar nebula, and they presumably would contain unique, highly refractory,
22 chemical signatures as a result. In addition, a primordial Vulcanoid population might have
23 affected Mercury’s surface chronology. Based on the size-frequency distribution of craters
24 on the Moon, Mars, Venus, and Mercury, it is thought that objects in the inner solar system
25 were resurfaced during the period of the Late Heavy Bombardment (LHB) 3.9 Gyr ago
26 (Strom et al. 2005). Vulcanoids removed from stable orbits in the Vulcanoid zone by non-
27 gravitational forces like the Yarkovsky effect (Vokrouhlický 1999; Vokrouhlický et al. 2000)
28 could have supplied a significant impactor population to Mercury after the LHB, making the
29 surface appear older (Leake et al. 1987; Head et al. 2007).

30 1.1. Early Searches

31 Le Verrier (1859) first proposed that a small planet, or collection of planets, interior to
32 Mercury could explain the observed precession of Mercury’s orbit. This hypothesized planet
33 was eventually given the name “Vulcan”, and numerous searches were conducted in an
34 attempt to find it. However, the proximity of intramercurial objects to the Sun makes them
35 difficult to observe from the Earth. To overcome the observational challenge of looking for
36 a faint object against a bright twilight sky, many of the early searches for the planet Vulcan

37 were conducted in the fleeting minutes of totality during solar eclipses. The first searches
38 for Vulcan were done visually, with obvious limitations. The first use of photographic plates
39 to search for an intra-Mercurial planet was by Perrine (1902), during the total solar eclipse
40 of May 18, 1901, on the island of Sumatra. After analyzing the plates from this expedition,
41 Perrine placed a limit of magnitude 5.0 (photographic) on the brightness of any planet
42 interior to Mercury and concluded that, “...there are probably no bodies of appreciable size
43 in the region close about the Sun, and that the cause of the disturbance in the motion of
44 Mercury must be sought elsewhere.” Subsequent observations during solar eclipses resulted
45 in an improved limiting magnitude of 8.0 (Perrine and Campbell 1907; Perrine 1909).

46 In 1915, Einstein (1915) showed that the precession of Mercury’s orbit could be explained
47 entirely by the then new theory of general relativity, thus eliminating the dynamical need for a
48 massive planet Vulcan. However, the question of whether there are any small bodies interior
49 to Mercury’s orbit remained unresolved. An archival search by Campbell and Trumpler
50 (1923) using photographic plates obtained during the solar eclipse of 1922 for the purpose
51 of measuring the deflection of starlight predicted by general relativity provided the tightest
52 constraint of all the early searches: a photographic magnitude of 8.5.

53 1.2. Modern Searches

54 More recently, Courten et al. (1976), summarizing a 10-year campaign to observe comets
55 during solar eclipses, reported, “...data which indicate the possible existence of one or more
56 relatively faint objects within twenty solar radii...and [ranging] from +9 to +7 in equiva-
57 lent visual magnitude”. Unfortunately, the nature of observing during total solar eclipses
58 precluded any direct follow-up observations of these possible detections. Since these re-
59 sults remain unpublished and have not been independently confirmed, it is difficult to assess
60 whether the claimed detections are real, and, if they are, whether the objects are Vulcanoids,
61 sungrazing comets (cf. Biesecker et al. (2002)), or some other type of body.

62 In contrast to all other published Vulcanoid searches, Leake et al. (1987) conducted a
63 search for Vulcanoids between 1979 and 1981 at $3.5 \mu\text{m}$. By virtue of operating in the
64 thermal infrared, this search was more sensitive to objects with low visual albedo. Leake et
65 al. estimated a detection probability of 75% for an object with an L-band magnitude of 5,
66 corresponding to an object diameter of 40-50 km. However, bad weather and the small field
67 of view (FOV) of their instrument limited their search to a total of 5.8 deg^2 within 1° of the
68 ecliptic—a small fraction of the Vulcanoid zone, as seen from Earth.

69 Prior to our work, the most complete search, in terms of depth and coverage, was

70 conducted by Durda et al. (2000), using data from the LASCO C3 coronagraph on the
71 SOHO spacecraft (Brueckner et al. 1995), which images a region from 0.02–0.14 AU (3.7–
72 30 solar radii). Durda et al., examined a 40-day sequence of LASCO C3 images. Except
73 for objects at the outer edge of the Vulcanoid zone with inclination $>25^\circ$, all dynamically
74 stable Vulcanoids should have passed through the instrument FOV during this period. No
75 Vulcanoids were found, down to detection limit of $V=8.0$. For objects with a Mercury-like
76 albedo and phase function (Veverka et al. 1988), this limit corresponds to a diameter of 22
77 and 65 km for objects at the inner and outer edges of the Vulcanoid zone (or 36-106 km for
78 an albedo of 0.05). Working independently, Schumacher and Gay (2001) also did not detect
79 any Vulcanoids in LASCO C3 images down to a limiting magnitude of $V=7$.

80 Subsequently, Durda and Stern (2003) conducted a Vulcanoid search using a visible
81 wavelength imaging system flown aboard NASA F/A-18B aircraft at an altitude of 49,000
82 feet. However, they were unable to improve upon the earlier Durda et al. (2000) results.

83 Merline et al. (2008) report preliminary results from their search for Vulcanoids using
84 the Wide Angle Camera (WAC) of the MESSENGER spacecraft’s Mercury Dual Imaging
85 System (MDIS), while the spacecraft was in cruise to Mercury. Spacecraft pointing restric-
86 tions limited observations to those with solar elongation $>30^\circ$, i.e., the outer 45% of the
87 Vulcanoid zone. No Vulcanoids were detected, down to a limiting magnitude of $V=8$, corre-
88 sponding to an Vulcanoid diameter of 15 km. Subsequent analysis of these observations has
89 brought this size limit down to 5 km, comparable to the results of our search (W. J. Merline,
90 private communication, 2012).

91 Finally, Zhao et al. (2009) report a Vulcanoid search using 15 cm telescopes equipped
92 with CCDs at two separate observatories in China during the 2008 total solar eclipse. They
93 found “three unidentified star-like objects” in images from both telescopes, but the relative
94 motion of these objects did not match that of a Vulcanoid. Both the angular size and
95 sensitivity of this search are unclear, although they report that stars as faint as $V=12.8$ were
96 detected.

97 2. HI-1 Data and Processing

98 For our search, we used archival data from the Heliospheric Imager (HI) instrument on
99 NASA’s STEREO spacecraft, available online from the STEREO Science Center (<http://stereo-ssc.nascom.nasa.gov>).
100 The Solar TERrestrial RELations Observatory (STEREO) mission is designed to study coro-
101 nal mass ejections (CMEs) from the Sun out to the orbit of the Earth and consists of two
102 nearly identical spacecraft. STEREO-A orbits the Sun slightly interior to Earth’s orbit,

103 while the other spacecraft, STEREO-B, orbits the Sun slightly exterior to Earth’s orbit
 104 (Kaiser et al. 2008). Seen from the Sun, the angular separation between the Earth and the
 105 two spacecraft increases by 22.5° per year. Our search focused on data from STEREO-A, as
 106 it has more stable pointing than STEREO-B.

107 The HI instrument, itself part of the Sun Earth Connection Coronal and Heliospheric
 108 Investigation (SECCHI), consists of two separate imagers: HI-1, with a 20° square FOV
 109 centered in the ecliptic plane at a solar elongation of 14° , and HI-2, with a 70° FOV centered
 110 on the ecliptic plane at a solar elongation of 53° (Eyles et al. 2009). The HI instruments
 111 use a series of baffles to prevent scattered light from the Sun from reaching the detector; as
 112 a result, HI is significantly more sensitive to faint targets like CMEs (or Vulcanoids) than
 113 traditional coronagraphic imagers. The HI-1A imager is particularly well-suited to searching
 114 for Vulcanoids, as all objects on dynamically stable orbits will be in the FOV at their eastern
 115 elongation, provided the following inequality is satisfied:

$$a\sqrt{1 - e^2} \cos i \gtrsim r \tan \beta \quad (1)$$

116 where a , e , and i are the semi-major axis, eccentricity, and inclination of the Vulcanoid’s
 117 orbit; $r \approx 0.97$ AU is the heliocentric distance of the STEREO-A spacecraft; and $\beta = 4^\circ$ is
 118 the angle between the sun and the inner edge of the FOV. This inequality is satisfied for all
 119 orbits with $a \geq 0.071$ AU, $e \leq 0.15$, and $i \leq 15^\circ$.

120 The HI-1 detector is a 2048×2048 pixel CCD. To obtain sufficient signal-to-noise (S/N)
 121 for observing faint CMEs, HI-1 typically integrates for 1200s. A single 1200s exposure would
 122 be significantly degraded by cosmic ray hits, which affect roughly 45 pixels s^{-1} (Eyles et al.
 123 2009). Instead, HI-1 typically acquires 30 separate 40-second exposures. Since the data vol-
 124 ume required to transmit all these images to Earth at full resolution would be prohibitive, the
 125 individual images are processed and combined onboard the spacecraft. The image processing
 126 includes a cosmic ray removal algorithm that compares each new image with the previous
 127 image on a pixel-by-pixel basis. If the value in a given pixel exceeds that in the previous
 128 image by more than 5σ , where σ is the predicted standard deviation based on the number
 129 of photoelectrons detected, that value is replaced with the value in the previous image. As
 130 seen from STEREO-A, the apparent motion of a Vulcanoid between 40s exposures is $\lesssim 5''$.
 131 Given the $35''$ size of the HI-1 pixels, a full-width at half-maximum value of the PSF of 3.34
 132 pixels in the X-direction and 2.96 pixels in the Y-direction (Bewsher et al. 2010), the rate of
 133 apparent motion for Vulcanoids, and that the signal from the solar F-corona is much brighter
 134 than the signal expected from a Vulcanoid, this cosmic ray removal algorithm does not affect
 135 the ability of the instrument to detect potential Vulcanoids.

136 After the cosmic ray removal, the bias level, as determined from a column in the CCD
 137 underscan region, is subtracted from the data and the images are binned by a factor of two.
 138 The resulting sequence of 1024×1024 pixel images are then summed and compressed using
 139 a lossless algorithm, and in general, only these processed, summed images are sent back to
 140 Earth. In normal operations, these 1200s combined images are obtained with a cadence of
 141 40 minutes.

142 2.1. Image Processing

143 HI data are available in three levels of processing: L0, L1, and L2. L0 data consists
 144 of the raw, uncalibrated image data. L1 data have been processed to correct for flat-field
 145 effects, image alignment, and the shutterless readout. As shown in panel A of Fig. 1, both
 146 L0 and L1 data are dominated by light scattered from the solar F-corona (zodiacal light).
 147 In a typical 40×40 pixel region near the right-hand edge of the image, the median value is
 148 118 DN/s. The signal from the F-corona is fairly stable with time, so it can be effectively
 149 removed from the data by subtracting a composite image formed from data taken over a
 150 sufficiently long baseline. In the L2 data, the composite image to be subtracted is created by
 151 averaging over the lowest 25% of pixel values obtained during either a 1- or 11-day running
 152 window at each pixel in the image. The result of L2 processing can be seen in panel B of
 153 Fig. 1. The same 40×40 pixel region has a median value of 0.2 DN/s in the L2 data. We
 154 used L2 data from the HI-1 instrument of STEREO-A (henceforth HI-1A) with the 11-day
 155 running window in our search.

156 With the F-corona effectively removed, CMEs and coronal streamers are readily appar-
 157 ent in the HI-1 data. Although the STEREO mission is designed to study solar phenomena
 158 such as these, for the purpose of searching for Vulcanoids they constitute an additional source
 159 of background “noise”. If not removed, this additional background, which is more significant
 160 at smaller angular distances from the Sun, will result in reduced sensitivity to Vulcanoids
 161 with small semi-major axes. We attempted to remove this two-dimensional, time-varying
 162 background from the L2 data by subtracting off the “sky” level in a circular annulus centered
 163 on each pixel. Based on an average PSF FWHM value of 1.57 pixels (binned), we adopted
 164 radii of 4.7 and 7.9 pixels ($3 \times$ and $5 \times$ the FWHM) for our sky background annulus. This
 165 method removes signal from diffuse features while preserving point sources. A sky-subtracted
 166 image is shown in panel C of Fig. 1. After this sky-subtraction, the median value in the
 167 40×40 region fell to 8×10^{-3} DN/s.

168 Since the pointing of the STEREO spacecraft was held fixed relative to the Sun, back-
 169 ground stars appear to drift through the HI-1 FOV. To facilitate the identification of objects

170 moving relative to the inertial frame, we co-registered all sky-subtracted L2 data obtained
 171 during a two-day window (typically a series of 72 images). The first image in the sequence
 172 was used to define an astrometric reference frame. We then calculated centroid positions
 173 for several hundred stars common to both images and used these to derive a third degree,
 174 two-dimensional polynomial transform that maps the second image into the frame of the
 175 reference image. This polynomial technique handles optical distortions near the edges of
 176 the instrument FOV better than a simple linear shift. After the data were co-registered, we
 177 subtracted a 9-image running median from each image to reduce the signal from any sources
 178 that remained fixed in inertial coordinates, e.g., stars. An example of the final processed
 179 image is shown in panel D of Fig 1.

180 2.2. Synthetic Vulcanoids

181 To quantify the detection efficiency of our search, we generated a population of 101
 182 synthetic Vulcanoids and added them to the L2 HI-1A data, with the appropriate level of
 183 Poisson noise, before our additional image processing. The orbital properties of the synthetic
 184 Vulcanoids were chosen to mimic those of the putative Vulcanoid population. During the
 185 search, the observers knew that synthetic Vulcanoids were present in the data, but they
 186 did not know where the synthetic objects were, how many objects were in a given image
 187 (between 23 and 42 with an average of 33), or whether a given object that was detected was
 188 real or synthetic.

189 Each of the 101 synthetic Vulcanoids was randomly assigned a value for the longitude of
 190 its ascending node, argument of periapsis, and mean anomaly at epoch. Given the FOV of
 191 the HI-1A instrument, we limited the range of orbital eccentricities to 0–0.15 and inclinations
 192 to 0–15°, with the value for each chosen randomly. Prior work by Stern and Durda (2000) has
 193 also shown that Vulcanoids are more likely to be found on highly circular orbits near the outer
 194 edge of the Vulcanoid zone. For the synthetic population as a whole, $\langle e \rangle = 0.07$ and $\langle i \rangle = 7.7^\circ$.
 195 Half of the synthetic Vulcanoids were given a semi-major axis randomly-distributed between
 196 0.07–0.14 A.U.; the other half were given semi-major axes distributed randomly between
 197 0.14–0.21 A.U. For each image to be examined, we calculated the positions of the synthetic
 198 objects in detector coordinates, and if the object was within the instrument field of view, we
 199 added a 2-D Gaussian PSF (FWHM of 1.67 pixels in the X-dimension and 1.48 pixels in the
 200 Y-dimension) with Poisson noise to the image. The positions of the synthetic Vulcanoids, in
 201 detector coordinates, over the 40-day search period are shown in Fig 2.

202 The apparent brightness of some Vulcanoids can change by nearly three orders of mag-
 203 nitude as they move through the HI-1A field of view. This is primarily a result of the large

204 range of phase angles at which they can be observed (roughly 20°-160° for a Vulcanoids in
 205 the outer Vulcanoid zone and 60°-120° for Vulcanoids in the inner Vulcanoid zone) as well
 206 as potentially significant changes in the object’s heliocentric distance and distance to the
 207 STEREO-A spacecraft while they are in the field of view. The synthetic Vulcanoids were
 208 assumed to be spherical and within each group ($a \leq 0.14$ AU and $a > 0.14$ AU), they were
 209 assigned diameters that uniformly spanned the range of 0.7–50 km, in logarithmically-spaced
 210 steps. The total signal (in DN/s) from each synthetic Vulcanoid was calculated according
 211 to the following equation:

$$F = \frac{\mu A d^2}{16 r_0^2 r^2 \Delta^2 G} \int \left(\frac{\lambda}{hc} \right) S_{\odot}(\lambda) R(\lambda, \alpha) H(\lambda) d\lambda \quad (2)$$

212 where A is the collection area of HI-1A ($A = \pi d_i^2/4$ where $d_i = 1.59$ cm), d is the diameter of
 213 the Vulcanoid in km, $r_0 = 1.496 \times 10^8$ km is the astronomical unit (AU), r is the heliocentric
 214 distance of the Vulcanoid in AU, Δ is the distance from STEREO-A to the Vulcanoid in AU,
 215 G is the system gain (15 photoelectrons / DN), λ_n/hc is the number of photons of wavelength
 216 λ_n per erg, S_{\odot} is the solar flux at 1 AU in $\text{erg s}^{-1} \text{cm}^{-2} \text{nm}^{-1}$, R is the absolute reflectance
 217 of the Vulcanoid at λ_n and phase angle α , and $H(\lambda_n)$ is the instrument response (which
 218 includes the CCD quantum efficiency). Finally, $\mu = 0.93$ is the correction factor for HI-1A
 219 between the theoretically predicted counts and counts actually measured (Bewsher et al.
 220 2010). Eq. 2 is integrated between 300–1100 nm, the range over which HI-1 is sensitive. The
 221 instrument response curve of HI-1A, $H(\lambda_n)$, contains a broad central peak from 600–750 nm,
 222 roughly similar to the Johnson R filter. However, there are significant side bands at 400 nm
 223 and 950 nm (cf. Fig. 6 in Bewsher et al., 2010). For an object with a Mercury-like spectrum,
 224 roughly 90% of the detected flux will be in the central pass band, 4% in the 400 nm side
 225 band, and 6% in the 950 nm side band.

226 The solar spectrum, S_{\odot} , was obtained from the HST CALSPEC database (Bohlin
 227 2007). The synthetic Vulcanoids were assumed to have spectral reflectance properties iden-
 228 tical to that of the planet Mercury, except with 1/3 the albedo, i.e., scaled to $p_R =$
 229 0.047 (Warell and Bergfors 2008). This albedo is comparable to that of C-type asteroids
 230 (Tholen and Barucci 1989). For objects with a different albedo, $d \propto p_R^{-1/2}$. The absolute
 231 reflectance of Mercury, as measured by the MDIS and MASCS instruments on the MESSEN-
 232 GER spacecraft at 11 wavelengths between 428–1013 nm at 5 phase angles from 35°–129° by
 233 Holsclaw et al. (2010) is shown in Fig. 3. For wavelengths between 300–428 nm and 1013–
 234 1100 nm, we linearly extrapolate the MDIS/MASCS data. For reflectances at phase angles
 235 between 35°–129°, we interpolate the MDIS/MASCS data, while for phase angles between
 236 20°–35°/129°–160° we scale the reflectance spectrum at 35°/129° by the V-band Mercury
 237 phase function of Mallama et al. (2002). Although we have used Mercury’s reflectance spec-

238 trum in our analysis, our results are insensitive to the choice of spectrum for reasonable solar
239 system alternatives, such as typical S- or C-type asteroids, when that spectrum is scaled to
240 an R-band albedo of 0.047.

241 3. Search Technique

242 After processing the data and adding synthetic Vulcanoids as described above, we cre-
243 ated movies from the images obtained during a two-day period. We then looped this movie
244 back and forth, at variable frame rates, while visually searching for moving objects. When
245 an object was found, the observer marked its position in one or more frames of the movie.
246 This technique takes advantage of the ability of the human eye to detect motion; very often
247 an object that was easily identifiable while cycling through the movie would be virtually in-
248 distinguishable from background noise when looking at an individual image. After searching
249 through all of the movies, the list of marked objects for each movie was compared to the
250 positions of the synthetic Vulcanoids and main belt asteroids in that movie. Even with a
251 population of just 101 synthetic Vulcanoids, with $70''$ pixels, there were multiple instances
252 in which there were two synthetic Vulcanoids within a five-pixel radius of a marked posi-
253 tion. These were automatically flagged for further review. Unless it was clear that both
254 objects were marked in the same frame, only the brighter of the two synthetic Vulcanoids
255 was recorded as being detected. Any marked position not matching the location of a syn-
256 thetic Vulcanoid or main belt asteroid was flagged for further inspection. With one exception
257 (discussed in Section 4.3), these were subsequently determined to be false positives—usually
258 the result of a interpolating a single “warm” pixel or a spurious grouping of random noise.

259 Although there are now several years of STEREO HI-1 data, the labor-intensive nature
260 of our search technique placed practical limitations on the amount of data that could be ana-
261 lyzed. The longest synodic period between an object in a dynamically stable Vulcanoid orbit
262 (i.e. having a semi-major axis < 0.21 AU) and an observer at 1 AU is 39 days. We therefore
263 selected a 40-day period from 2008-12-10 to 2009-01-19 to examine in our search, based on
264 the low solar activity and avoidance of the galactic center. (We had previously examined the
265 40-day period from 2009-01-19 to 2009-03-01 and found no Vulcanoids (Steffl et al. 2010),
266 but we used a less effective sky subtraction technique resulting in a less sensitive search than
267 the one described in this paper). For any given 40-day period, a Vulcanoid at the outer edge
268 of the Vulcanoid zone will spend roughly 15 days continuously in the HI-1A field of view
269 during its single pass through elongation. In contrast, a Vulcanoid at the inner edge of the
270 Vulcanoid zone will spend roughly 30 hours in the HI-1A FOV per elongation, but will pass
271 through elongation 5 or 6 times.

272 As has been pointed out by many others before us, given a careful observer, the human
273 eye is often better at finding low S/N point sources with fewer false positives than automated
274 search algorithms. This is especially true given the relatively dense stellar backgrounds in the
275 HI-1 images and the large range of apparent motions that Vulcanoids can exhibit (anywhere
276 from no apparent motion at all up to a few hundred arcseconds per hour, positive or negative,
277 in both right ascension and declination). However, using human observers to manually look
278 for Vulcanoids introduces a certain stochastic element to the search. To minimize the chance
279 that a faint Vulcanoid might be missed due to observer fatigue or random chance, each movie
280 was independently examined by four separate observers (AJS, NJC, ABS, and DDD).

281 Finally, we note that based on this work and previous searches, e.g. the search for
282 small satellites of Pluto of Steffl et al. (2006), adding synthetic objects to the data not only
283 provides a quantitative means of estimating the detection efficiency but actually results in
284 a more sensitive search. The tedium of searching through large numbers of images for point
285 sources marginally brighter than the background while failing to find any can quickly lead
286 to observer fatigue and a less thorough search. However, the simple positive reinforcement
287 of finding an object in the data, whether synthetic or not, can help keep a human observer
288 focused on the search, despite its repetitive nature.

289 4. Results

290 No Vulcanoids were detected in our search. Although we did not detect any Vulcanoids,
291 we observed a variety of other solar system objects: the planets Mercury, Venus, Uranus, and
292 Neptune; the comet 67P/Churyumov-Gerasimenko; more than 30 Kruetz-family sungrazing
293 comets (Biesecker et al. 2002); the non-group sungrazing comets C/2008 Y12 (SOHO) and
294 C/2009 A1 (STEREO); and numerous main-belt asteroids, some as faint as $V=13.8$, as
295 determined by the JPL HORIZONS ephemeris (Giorgini et al. 1996). In addition, 58 of
296 the 101 synthetic Vulcanoids added to the data were detected by at least one of the four
297 observers, which we use to place upper limits on the size of any putative Vulcanoids. Finally,
298 as discussed below, we initially classified the sun-grazing comet C/2008 Y12 (SOHO) as a
299 candidate Vulcanoid. This resulted in an additional search through all images from the
300 HI-1 instruments on both STEREO-A and STEREO-B over the period from 2008-12-08 to
301 2009-03-01. We found no Vulcanoids in this additional search but cannot place quantitative
302 limits on this additional non-detection, as no synthetic Vulcanoids were added.

4.1. Insensitivity to Orbital Parameters

The detection efficiency of Vulcanoids, whether real or synthetic, will clearly be a strong function of the object’s size, as the larger the object, the brighter it appears. It is also possible that our search might be biased towards detecting objects with a certain range of orbital parameter values. For example, in our prior Vulcanoid search we found that given two synthetic Vulcanoids of the same size, the one with the greater orbital semi-major axis was more likely to be detected (Steffl et al. 2010). To identify whether any such biases were present in our current search, we plot the orbital parameters of the synthetic Vulcanoid population as a function of diameter in Figs. 4 and 5. Synthetic Vulcanoids that were detected by at least one observer have filled symbols and those that were not detected at all have open symbols. From these figures, it is immediately clear that there is an extremely strong dependence on object size, with all 57 synthetic Vulcanoids larger than 5 km in diameter being detected by at least one observer and only 1 of the 44 synthetic Vulcanoids smaller than 5 km in diameter being detected (and then, only by one observer). However, there is no obvious correlation between whether an object was detected and any of its orbital parameters.

To quantitatively verify our search’s insensitivity to a Vulcanoid’s orbital parameters, we divided the synthetic Vulcanoids into two populations based on whether they were detected or not and conducted a series of statistical tests. These are described in more detail in the Appendix. None of these tests showed any significant deviations from a random uniform distribution or correlations between pairs of parameters. This is a somewhat surprising result. Evidently the sky annulus subtraction technique described in Section 2.1, has removed the bias towards detecting objects with larger semi-major axes observed in our initial search. Given the relatively low number of synthetic Vulcanoids (101), it was not possible to investigate whether any statistically significant groupings of three or more orbital parameters exist.

4.2. Detection Efficiency vs. Object Size

We present the number of synthetic Vulcanoid detections for each observer, X_{obs} , as a function of size in Table 1. We have grouped the objects into 13 size bins, corresponding to a factor of $\sqrt{2}$ in diameter. As might be expected, there is some disparity between the detection rates of the four observers, with observer 1 detecting 58 of the 101 synthetic Vulcanoids and observer 4 detecting 50 of the 101 synthetic Vulcanoids. Surprisingly, though, all the differences between the observers occurred for objects 4-8 km diameter. All four observers detected all 45 objects larger than 8 km and none of the 38 objects smaller than 4 km. For

337 each observer, the detection efficiency, ϵ , in a given size bin is simply X_{obs}/N . We plot ϵ for
 338 each of the four individual observers as well as ϵ_{avg} , the average detection efficiency of all
 339 observers vs. object diameter in Fig. 6. 1σ confidence intervals for the ϵ_{avg} are derived from
 340 Monte Carlo analysis, as described below. We find $\epsilon_{avg} = 0.800^{+0.057}_{-0.067}$ (32/40) for objects
 341 between 5.7-8.0 km diameter and $\epsilon_{avg} = 0.125^{+0.065}_{-0.051}$ (4/32) for objects between 4.0-5.7 km.
 342 Given the individual detection efficiencies, we calculate the probability, P_{det} , that at least
 343 one of the four observers would detect a single object, as a function of size. Subject to the
 344 assumptions stated in Section 2.2 (namely a R-band Vulcanoid albedo of $p_R=0.05$) we find
 345 that our search should have detected all Vulcanoids larger than 5.7 km in diameter. However
 346 this approach ignores the statistical uncertainty in the observed values of ϵ , which arises from
 347 the small number of synthetic Vulcanoids in each size bin.

348 We use a Monte Carlo model to quantitatively determine the effect of statistical uncer-
 349 tainty on our limits. For each size bin and observer (or the sum of the four observers, in the
 350 case of ϵ_{avg}) we set the detection efficiency, ϵ , equal to a pseudo-random number generated
 351 over the interval $[0, 1]$, inclusive. Using the probability mass function for the binomial dis-
 352 tribution, we calculated the probability of detecting exactly X_{obs} synthetic Vulcanoids, given
 353 N Vulcanoids in the size bin and ϵ . We then generated a second pseudo-random number
 354 between 0 and 1, and if it was less than or equal to this probability the test was considered
 355 successful at reproducing the observations and we recorded the value of ϵ . This process
 356 was repeated until 10^6 values for ϵ were recorded. 1σ confidence intervals were produced by
 357 sorting the recorded values of ϵ into ascending order and finding the minimum contiguous
 358 interval ($\epsilon_{high} - \epsilon_{low}$) that contained 68.3% of the ϵ values. These confidence intervals are
 359 shown in Table 1.

360 To determine the probability that a single Vulcanoid would be detected by at least one
 361 observer, we randomly selected one of the recorded values for ϵ for each observer and tested
 362 whether this value was less than or equal to a pseudo-random number, i.e. if that observer
 363 failed to detect the object. If this test was true for all four observers, the Vulcanoid escaped
 364 detection. We repeated this 10^6 times and counted the total number of times the Vulcanoid
 365 was detected. The probability of a single Vulcanoid being detected by least one observer,
 366 given statistical uncertainties, P'_{det} , is shown in Table 1. We note that the values for P'_{det}
 367 are significantly higher than P_{det} for Vulcanoids below 5.7 km in diameter. This is due to
 368 the fact that, given the small values for N , even if $X_{obs} = 0$, it is not possible to exclude
 369 a non-zero value for ϵ with a high degree of confidence. For example, observer 4 detected
 370 0 of 8 objects between 4.0-5.7 km, but even a value of $\epsilon = 0.31$ would yield this result 5%
 371 of the time. Thus, when at least one observer has an observed detection efficiency, ϵ , close
 372 to zero, P'_{det} is likely too high. The converse is also true: when at least one observer has
 373 ϵ close to unity, P'_{det} is likely an underestimate. With this in mind, we are able to place

374 a 3σ upper limit (i.e., a confidence level >0.997) on the existence of any Vulcanoids larger
 375 than 5.7 km in diameter. As stated above, our size limits are dependent on the value of the
 376 R-band albedo, $p_R = 0.05$, we assumed for Vulcanoids. If the actual albedo of Vulcanoids is
 377 different from this value, our diameter limits scale as $p_R^{-1/2}$.

378 4.3. C/2008 Y12 (SOHO)

379 In our search, we found one object that did not correspond to a synthetic Vulcanoid
 380 or any known object in the IAU Minor Planet Centers database (Gareth Williams, private
 381 communication, 2011). This object was first detected in an image from 2008-12-21T17:44 UT
 382 and appeared in 15 consecutive HI-1A images before its apparent motion carried it outside
 383 the instrument’s FOV. Although the object’s motion was similar to several to the synthetic
 384 Vulcanoids, it appeared somewhat diffuse and brightened as it moved closer to the sun. We
 385 thus suspected that this candidate Vulcanoid might be a previously undetected sungrazing
 386 comet. However, given the short 9.3-hour arc and $70''$ pixels it was not possible to obtain
 387 a unique orbital solution. We therefore began a concerted effort to see if the object could
 388 be re-acquired in images from the HI-1 instruments on either STEREO-A or STEREO-B
 389 obtained over the 83-day period from 2008-12-08 to 2009-03-01. These data were processed
 390 and searched using the techniques described above, but without the addition of any synthetic
 391 Vulcanoids. Ultimately, we were not able to reacquire the object and no other candidate
 392 Vulcanoids were detected. Since we were specifically looking to reacquire the candidate
 393 object in the data, this secondary search was likely not as sensitive to Vulcanoids in general
 394 as our primary search. However, lacking any synthetic Vulcanoids to detect, we can not
 395 quantitatively verify this hypothesis. Given that in our primary search, all four observers
 396 detected all 45 synthetic objects larger than 8 km, it seems likely that were such an object
 397 present in this extended data set, it would have been detected. This gives us additional
 398 confidence that some unknown systematic effect unique to either the HI-1A or the time
 399 period from 2008-12-10 to 2009-01-19 is not preventing the detection of a real Vulcanoid.

400 Subsequently, we learned of the comet C/2008 Y12 (SOHO), which was discovered in
 401 7 images from the LASCO C2 coronagraph on the SOHO spacecraft, starting on 2008-12-
 402 22T16:54—less than 14 hours after the Vulcanoid candidate was last seen in the HI-1A images.
 403 The predicted positions of C/2008 Y12 (SOHO) in the HI-1A images using the initial orbital
 404 fit (Marsden 2009) were not a good match to our candidate object. However, we were able
 405 to find a single set of orbital parameters that yielded average positional residuals of $37''$ for
 406 the Vulcanoid candidate in the STEREO HI-1A images and $3''$ for C/2008 Y12 (SOHO) in
 407 the SOHO LASCO-C2 images—less than half the size of the respective detector pixels. After

408 reporting these results to the IAU Minor Planet Center, a new orbital fit was published
 409 Williams (2012). However, this published fit assumed an eccentricity of 1.0, and as a result,
 410 it is significantly less accurate than our orbital fit shown in Table 2.

411 5. Discussion

412 Although it is dynamically stable, the Vulcanoid zone is in a rough neighborhood.
 413 It occupies a comparatively small volume of space and due to its proximity to the sun,
 414 orbital velocities are large. Leake et al. (1987) and Stern and Durda (2000) showed that even
 415 for a wide variety of assumptions about the size and material properties of a hypothetical
 416 population, Vulcanoids will experience significant collisional disruption and erosion unless
 417 the mean orbital eccentricity of the population is extremely small ($\sim 10^{-3}$). However,
 418 dynamical studies by Evans and Tabachnik (2002) showed that test particles between 0.09
 419 and 0.20 AU on initially circular orbits with zero inclination evolved dynamically such that,
 420 after just 100 Myr, the population had a mean eccentricity of $\langle e \rangle = 0.0935$ and a mean
 421 maximum eccentricity over the 100 Myr of $\langle e_{max} \rangle = 0.15$. This increase in mean eccentricity
 422 is due to the interaction of various orbital resonances with Mercury as its orbit evolved
 423 over the simulation. For a Vulcanoid population with mean eccentricity of $\langle e \rangle = 0.0935$,
 424 typical encounter velocities between Vulcanoids will be in the range of 10-20 km s⁻¹ and
 425 collisional disruption/erosion is extremely efficient. For an initial Vulcanoid population with
 426 a power-law index of -2.5, 300 objects larger than 1 km radius, and $\langle e \rangle = 0.1024$, high-
 427 energy collisions with small bodies reduced all objects to debris, no larger than 1 km radius,
 428 in 1.2 Gyr (Stern and Durda 2000). For an initial population of 10^4 objects with $r > 1$ km,
 429 this collisional destruction timescale was just 1.6 Myr.

430 However, radiative transport mechanisms like the Yarkovsky effect would have quickly
 431 removed the smaller collisional remnants. In simulations by Vokrouhlický et al. (2000) all
 432 Vulcanoids 1 km in diameter and smaller were removed from the Vulcanoid zone by Yarkovsky
 433 drift, with typical lifetimes of 100 Myr for 0.1 km objects and 500 Myr for 1 km objects.
 434 Even objects up to 10 km in size showed strong depletion (80%–100%) over the age of the
 435 solar system. By removing the small body population, the Yarkovsky effect might greatly
 436 reduce the efficiency of collisional erosion in the Vulcanoid zone. To date, there have been
 437 no studies combining the effects of collisional evolution and Yarkovsky drift in the Vulcanoid
 438 zone.

439 If we assume that the present-day Vulcanoid population both exists and obeys a steady-
 440 state collisional fragmentation size distribution, $dn = C * r^{-3.5} dr$ (Dohnanyi 1969; Williams and Wetherill
 441 1994), then our 3σ upper limit implies that no more than 76 primordial Vulcanoids remain in

442 the Vulcanoid zone—the last remnants of a much larger initial population. Such Vulcanoids
443 would all be larger than 1 km in diameter, as primordial objects smaller than this will have
444 been removed from the Vulcanoid zone by Yarkovsky drift. However, since the combination
445 of collisional evolution and Yarkovsky drift could result in either the complete depletion of
446 a primordial Vulcanoid population or something less than that, our upper limits cannot be
447 extrapolated to place any meaningful constraints on a hypothetical primordial Vulcanoid
448 population.

449 Finally, we note that if a Vulcanoid is subsequently discovered (hopefully below our de-
450 tection limits) it is possible that it may be a scattered Near-Earth Object (NEO) rather
451 than a primordial Vulcanoid. Recent modeling of the orbital distribution of NEOs by
452 Greenstreet et al. (2012) suggests that up to 0.006% of the NEO population might end
453 up in orbits with an aphelion interior to Mercury’s aphelion. Given that limit, an NEO
454 interloper might have an absolute magnitude as low as $H \simeq 21$, corresponding to a diameter
455 between 170-370 m, more than an order of magnitude smaller than the detection limits of
456 our search.

457 We kindly thank D. Bewsher for providing the instrument response curves for STEREO
458 HI-1, G. M. Holsclaw for providing the absolute reflectance of Mercury as measured by
459 MASCS/MDIS, T. V. Spahr for initial orbital solutions for the object that turned out to
460 be C/2008 Y12 (SOHO), and K. Battams for discussions about C/2008 Y12 (SOHO) and
461 its orbit. Support for this work was provided by NASA Planetary Geology and Geophysics
462 program through grant NNX09AD65G.

463 A. Statistical Tests

464 To determine if there were any statistically significant deviations in the detected and/or
465 non-detected populations of synthetic Vulcanoids, we conducted a series of statistical tests.
466 The first test was to divide the range of possible values for each orbital parameter into four,
467 equally-spaced bins. If the parameter values are randomly distributed, then the expectation
468 is that 1/4 of the total population should have parameter values in the range covered by
469 each bin. The cumulative binomial distribution can be used to determine the significance
470 of any deviation from this expected value. The largest deviation from a random uniform
471 distribution occurred in the non-detected population: the fourth semi-major axis bin had 17
472 objects, compared to an expectation value of 10.75—an event with only a 2.5% probability.
473 While this may seem marginally significant, given that we conducted 24 separate tests, we
474 would expect one of them to have as large a deviation nearly 46% of the time. Thus, we

475 conclude there were no statistically significant deviations from a random normal distribution.

476 We also performed one- and two-sample Kolmogorov-Smirnoff (K-S) tests on the dis-
477 tributions of orbital parameters for both the detected and undetected populations. A one-
478 sample K-S test compares the empirical distribution function of a sample population with
479 the cumulative distribution function of a reference distribution (in this case, a random uni-
480 form distribution) and evaluates the significance of any deviations. None of the empirical
481 distribution functions of the six orbital parameters for either of the two populations was
482 significantly different from a random uniform distribution. Similarly, a two-sample K-S test
483 compares the empirical distribution functions of two sample populations to determine if they
484 are consistent with being derived from the same parent distribution. We found no statisti-
485 cally significant difference between the parent distributions of the detected and non-detected
486 populations for any of the six orbital parameters.

487 Finally, we examined each of the 21 combination of the six orbital parameters and
488 Vulcanoid diameter for both possible correlations. Both the Pearson linear correlation coef-
489 ficient (which measures how well two variables are linearly related) and the Spearman rank
490 correlation coefficient (which measures how well the relationship between the two variables
491 can be described using a monotonic function) exhibited near-zero values for all parameter
492 combinations.

493 REFERENCES

- 494 Bewsher, D., Brown, D. S., Eyles, C. J., Kellett, B. J., White, G. J., Swinyard, B., Jul.
495 2010. Determination of the Photometric Calibration and Large-Scale Flatfield of the
496 STEREO Heliospheric Imagers: I. HI-1. *Sol. Phys.*264, 433–460.
- 497 Biesecker, D. A., Lamy, P., St. Cyr, O. C., Llebaria, A., Howard, R. A., Jun. 2002. Sungraz-
498 ing Comets Discovered with the SOHO/LASCO Coronagraphs 1996-1998. *Icarus*157,
499 323–348.
- 500 Bohlin, R. C., Apr. 2007. HST Stellar Standards with 1% Accuracy in Absolute Flux. In:
501 Sterken, C. (Ed.), *The Future of Photometric, Spectrophotometric and Polarimetric*
502 *Standardization*. Vol. 364 of *Astronomical Society of the Pacific Conference Series*. p.
503 315.
- 504 Brueckner, G. E., Howard, R. A., Koomen, M. J., Korendyke, C. M., Michels, D. J., Moses,
505 J. D., Socker, D. G., Dere, K. P., Lamy, P. L., Llebaria, A., Bout, M. V., Schwenn,
506 R., Simnett, G. M., Bedford, D. K., Eyles, C. J., Dec. 1995. The Large Angle Spec-
507 troscopic Coronagraph (LASCO). *Sol. Phys.*162, 357–402.

- 508 Campbell, W. W., Trumpler, R., Aug. 1923. Search for Intramercurial Bodies. *PASP*35, 214.
- 509 Campins, H., Davis, D. R., Weidenschilling, S. J., Magee, M., 1996. Searching For Vulcanoids.
510 In: T. Rettig & J. M. Hahn (Ed.), *Completing the Inventory of the Solar System*.
511 Vol. 107 of *Astronomical Society of the Pacific Conference Series*. pp. 85–96.
- 512 Courten, H. C., Brown, D. W., Albert, D. B., Sep. 1976. Summary Paper: Ten Years of Solar
513 Eclipse Comet Searches. In: *Bulletin of the American Astronomical Society*. Vol. 8 of
514 *Bulletin of the American Astronomical Society*. p. 504.
- 515 Dohnanyi, J. S., May 1969. Collisional Model of Asteroids and Their Debris. *J. Geo-*
516 *phys. Res.*74, 2531.
- 517 Durda, D. D., Stern, S. A., May 2003. High-altitude searches for vulcanoids: Observations
518 from F/A-18B aircraft. In: *AAS/Division for Planetary Sciences Meeting Abstracts*
519 *#35*. Vol. 35 of *Bulletin of the American Astronomical Society*. p. 981.
- 520 Durda, D. D., Stern, S. A., Colwell, W. B., Parker, J. W., Levison, H. F., Hassler, D. M., Nov.
521 2000. A New Observational Search for Vulcanoids in SOHO/LASCO Coronagraph
522 Images. *Icarus* 148, 312–315.
- 523 Einstein, A., 1915. Erklärung der Perihelionbewegung der Merkur aus der allgemeinen Rel-
524 ativitätstheorie. *Sitzungsber. preuss.Akad. Wiss.*, vol. 47, No.2, pp. 831-839, 1915 47,
525 831–839.
- 526 Evans, N. W., Tabachnik, S., May 1999. Possible long-lived asteroid belts in the inner Solar
527 System. *Nature*399, 41–43.
- 528 Evans, N. W., Tabachnik, S. A., Jun. 2002. Structure of possible long-lived asteroid belts.
529 *MNRAS*333, L1–L5.
- 530 Eyles, C. J., Harrison, R. A., Davis, C. J., Waltham, N. R., Shaughnessy, B. M., Mapson-
531 Menard, H. C. A., Bewsher, D., Crothers, S. R., Davies, J. A., Simnett, G. M.,
532 Howard, R. A., Moses, J. D., Newmark, J. S., Socker, D. G., Halain, J.-P., Defise, J.-
533 M., Mazy, E., Rochus, P., Feb. 2009. The Heliospheric Imagers Onboard the STEREO
534 Mission. *Sol. Phys.*254, 387–445.
- 535 Giorgini, J. D., Yeomans, D. K., Chamberlin, A. B., Chodas, P. W., Jacobson, R. A., Keesey,
536 M. S., Lieske, J. H., Ostro, S. J., Standish, E. M., Wimberly, R. N., Sep. 1996. JPL’s
537 On-Line Solar System Data Service. *Bulletin of the American Astronomical Society*
538 28, 1158.

- 539 Greenstreet, S., Ngo, H., Gladman, B., Jan. 2012. The orbital distribution of Near-Earth
540 Objects inside Earth's orbit. *Icarus*217, 355–366.
- 541 Head, J. W., Chapman, C. R., Domingue, D. L., Hawkins, S. E., McClintock, W. E.,
542 Murchie, S. L., Prockter, L. M., Robinson, M. S., Strom, R. G., Watters, T. R.,
543 Aug. 2007. The Geology of Mercury: The View Prior to the MESSENGER Mission.
544 *Space Sci. Rev.*131, 41–84.
- 545 Holsclaw, G. M., McClintock, W. E., Domingue, D. L., Izenberg, N. R., Blewett, D. T.,
546 Sprague, A. L., Sep. 2010. A comparison of the ultraviolet to near-infrared spectral
547 properties of Mercury and the Moon as observed by MESSENGER. *Icarus*209, 179–
548 194.
- 549 Kaiser, M. L., Kucera, T. A., Davila, J. M., St. Cyr, O. C., Guhathakurta, M., Christian,
550 E., Apr. 2008. The STEREO Mission: An Introduction. *Space Sci. Rev.*136, 5–16.
- 551 Le Verrier, U. J., 1859. Theorie du mouvement de Mercure. *Annales de l'Observatoire de*
552 *Paris* 5, 1–195.
- 553 Leake, M. A., Chapman, C. R., Weidenschilling, S. J., Davis, D. R., Greenberg, R., Sep. 1987.
554 The chronology of Mercury's geological and geophysical evolution - The Vulcanoid
555 hypothesis. *Icarus* 71, 350–375.
- 556 Lebofsky, L. A., Jun. 1975. Stability of frosts in the solar system. *Icarus* 25, 205–217.
- 557 Mallama, A., Wang, D., Howard, R. A., Feb. 2002. Photometry of Mercury from
558 SOHO/LASCO and Earth. The Phase Function from 2 to 170 deg. *Icarus*155, 253–
559 264.
- 560 Marsden, B. G., Mar. 2009. Comets C/2008 Y10, 2008 Y11, 2008 Y12 (SOHO). *Minor Planet*
561 *Electron. Circ.* F17.
- 562 Merline, W. J., Chapman, C. R., Solomon, S. C., Chabot, N. L., Gold, R. E., Hawkins, S. E.,
563 Robinson, M. S., Sep. 2008. A Program to Search for Vulcanoids from MESSENGER.
564 In: AAS/Division for Planetary Sciences Meeting Abstracts #40. Vol. 40 of *Bulletin*
565 *of the American Astronomical Society.* p. 491.
- 566 Perrine, C. D., Oct. 1902. The Search for an Intra-Mercurial Planet at the Total Solar Eclipse
567 of 1901, May 18. *PASP*14, 160–163.
- 568 Perrine, C. D., 1909. The search for intramercurial bodies at the total solar eclipse of January
569 3, 1908. *Lick Observatory Bulletin* 5, 95–97.

- 570 Perrine, C. D., Campbell, W. W., 1907. Results of the search for an intramercurial planet
571 at the total solar eclipse of August 30, 1905. *Lick Observatory Bulletin* 4, 115–117.
- 572 Schumacher, G., Gay, J., Mar. 2001. An attempt to detect Vulcanoids with SOHO/LASCO
573 images. I. Scale relativity and quantization of the solar system. *A&A*368, 1108–1114.
- 574 Sekanina, Z., Chodas, P. W., Dec. 2005. Origin of the Marsden and Kracht Groups of
575 Sunskirting Comets. I. Association with Comet 96P/Machholz and Its Interplanetary
576 Complex. *ApJS*161, 551–586.
- 577 Steffl, A. J., Cunningham, N. J., Graps, A. L., Durda, D. D., Stern, S. A., Oct. 2010. A
578 Search for Vulcanoids Using STEREO Heliospheric Imager Data. In: *AAS/Division
579 for Planetary Sciences Meeting Abstracts #42*. Vol. 42 of *Bulletin of the American
580 Astronomical Society*. p. 1052.
- 581 Steffl, A. J., Mutchler, M. J., Weaver, H. A., Stern, S. A., Durda, D. D., Terrell, D., Merline,
582 W. J., Young, L. A., Young, E. F., Buie, M. W., Spencer, J. R., Aug. 2006. New
583 Constraints on Additional Satellites of the Pluto System. *AJ*132, 614–619.
- 584 Stern, S. A., Durda, D. D., Feb. 2000. Collisional Evolution in the Vulcanoid Region: Impli-
585 cations for Present-Day Population Constraints. *Icarus* 143, 360–370.
- 586 Strom, R. G., Malhotra, R., Ito, T., Yoshida, F., Kring, D. A., Sep. 2005. The Origin of
587 Planetary Impactors in the Inner Solar System. *Science* 309, 1847–1850.
- 588 Tholen, D. J., Barucci, M. A., 1989. Asteroid taxonomy. In: Binzel, R. P., Gehrels, T.,
589 Matthews, M. S. (Eds.), *Asteroids II*. pp. 298–315.
- 590 Veverka, J., Helfenstein, P., Hapke, B., Goguen, J. D., 1988. Photometry and polarimetry
591 of Mercury. pp. 37–58.
- 592 Vokrouhlický, D., Apr. 1999. A complete linear model for the Yarkovsky thermal force on
593 spherical asteroid fragments. *A&A*344, 362–366.
- 594 Vokrouhlický, D., Farinella, P., Bottke, W. F., Nov. 2000. The Depletion of the Putative
595 Vulcanoid Population via the Yarkovsky Effect. *Icarus* 148, 147–152.
- 596 Warell, J., Bergfors, C., Dec. 2008. Mercury’s integral phase curve: Phase reddening and
597 wavelength dependence of photometric quantities. *Planet. Space Sci.* 56, 1939–1948.
- 598 Williams, D. R., Wetherill, G. W., Jan. 1994. Size distribution of collisionally evolved aster-
599 oidal populations - Analytical solution for self-similar collision cascades. *Icarus*107,
600 117.

601 Williams, G. V., Jan. 2012. Observations and Orbits of Comets. Minor Planet Electronic
602 Circulars, 23.

603 Zhao, H., Lu, H., Zhaori, G., Yao, J., Ma, Y., Nov. 2009. The search for vulcanoids in the
604 2008 total solar eclipse. *Science in China G: Physics and Astronomy* 52, 1790–1793.

Table 1. Synthetic Objects Detected by Observer

Diameter (km) ^a	X _{obs1}	X _{obs2}	X _{obs3}	X _{obs4}	N	ϵ_{avg} ^b	P _{det}	P' _{det} ^c
0.7–1.0	0	0	0	0	4	0.000 ^{+0.065}	0.000	0.517 ^d
1.0–1.4	0	0	0	0	8	0.000 ^{+0.034}	0.000	0.344 ^d
1.4–2.0	0	0	0	0	10	0.000 ^{+0.028}	0.000	0.294 ^d
2.0–2.8	0	0	0	0	8	0.000 ^{+0.034}	0.000	0.344 ^d
2.8–4.0	0	0	0	0	8	0.000 ^{+0.034}	0.000	0.344 ^d
4.0–5.7	3	1	0	0	8	0.125 ^{+0.065} _{-0.051}	0.453	0.611 ^d
5.7–8.0	10	9	8	5	10	0.800 ^{+0.057} _{-0.067}	1.000	0.998
8.0–11.3	8	8	8	8	8	1.000 _{-0.034}	1.000	1.000
11.3–16.0	8	8	8	8	8	1.000 _{-0.034}	1.000	1.000
16.0–22.6	8	8	8	8	8	1.000 _{-0.034}	1.000	1.000
22.6–32.0	9	9	9	9	9	1.000 _{-0.031}	1.000	1.000
32.0–45.3	8	8	8	8	8	1.000 _{-0.034}	1.000	1.000
45.3–64.0	4	4	4	4	4	1.000 _{-0.065}	1.000	0.999

^aDiameter assumes a Vulcanoid R-band albedo of 0.05. For other assumed values of the albedo, $d \propto p_R^{-1/2}$.

^bDetection efficiency, averaged over the four observers, with 1σ (68.3%) confidence intervals.

^cProbability of at least one of the four observers detecting a single object, given statistical uncertainties associated with X_{obs} detections of N objects for each observer.

^dWhen X_{obs}=0 for at least one observer, P'_{det} is likely to significantly overstate the detection probability. This results from the fact that given the small value of N, a non-zero value for ϵ_{obs} cannot be excluded with a high degree of confidence, even though in all likelihood, $\epsilon \approx 0$

Table 2. Orbital Elements for C/2008 Y12 (SOHO)

Orbit Solution	q (AU)	e	i (°)	Ω (°)	ω (°)	T ₀ (UTC)
Marsden (2009)	0.0533	1.0	154.34	35.03	140.06	2008 Dec. 22.65
Williams (2012)	0.0658983	1.0	23.39475	312.10406	145.62274	2008 Dec. 22.60543
This work	0.0659134	0.970428	23.38917	312.10392	146.56106	2008 Dec. 22.62134

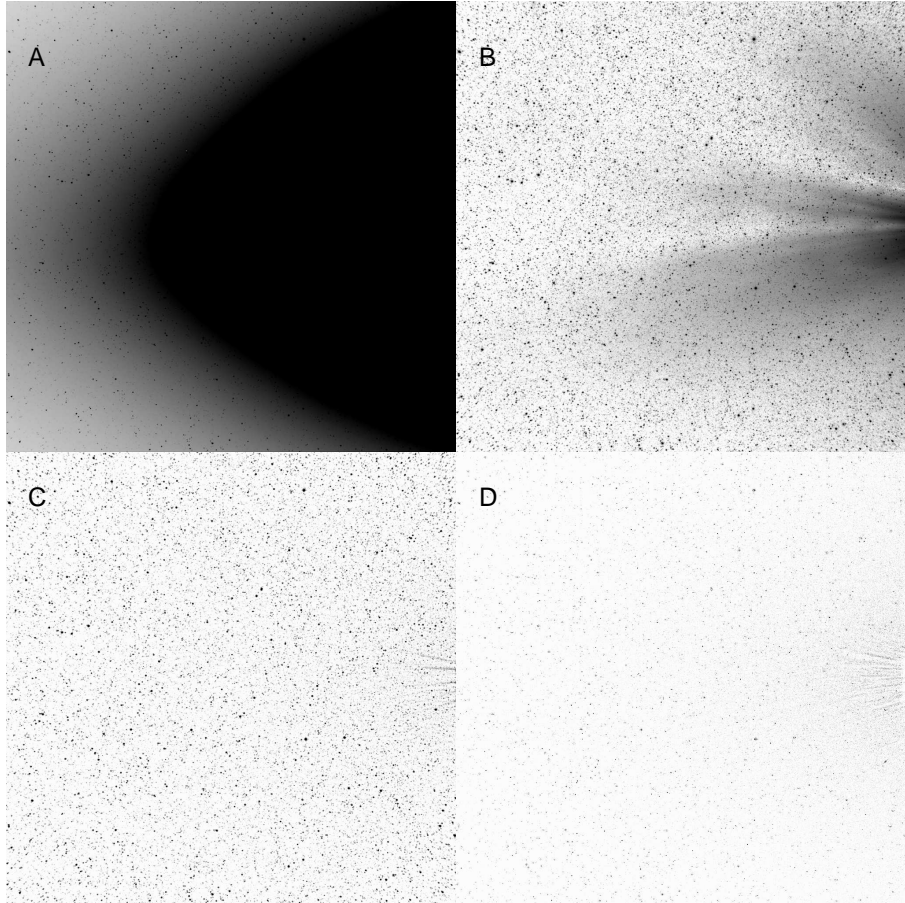


Fig. 1.— STEREO HI-1A images at various levels of processing using the same stretch. Panel A shows an image after Level 1 processing. The solar F-corona (zodiacal light) dominates the image. Panel B shows the same image after Level 2 processing to remove the solar F-corona. Streamers and other features of solar origin are clearly visible. All point-like sources are stars. Panel C shows the Level 2 image in panel B after our additional sky subtraction; the solar features have been almost completely removed. Panel D shows the image in panel C after subtracting the median of the aligned images to suppress sources that are fixed in inertial coordinates (e.g. stars). See the text in Section 2.1 for more details.

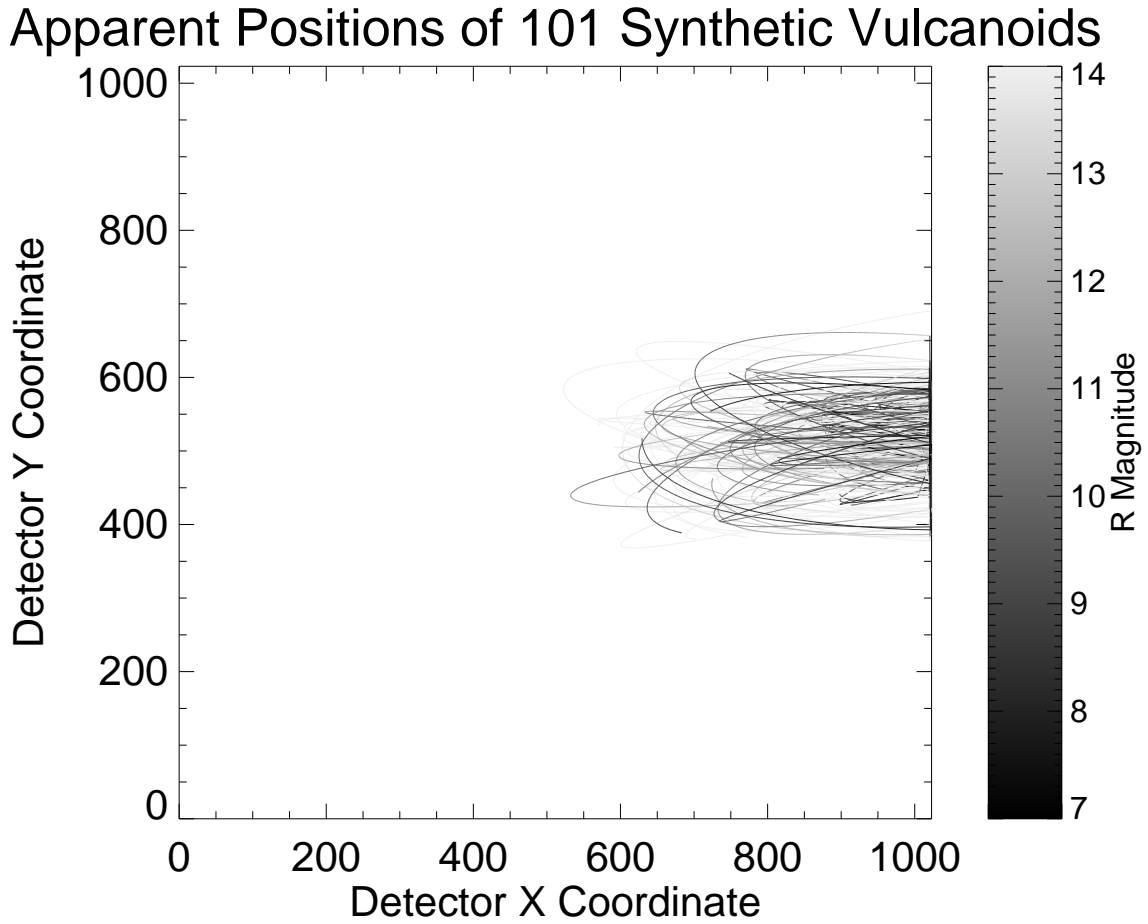


Fig. 2.— Positions of the synthetic Vulcanoid population in HI-1A detector coordinates during the 40-day search period. Shades of gray indicate the instantaneous apparent R magnitude of the synthetic object.

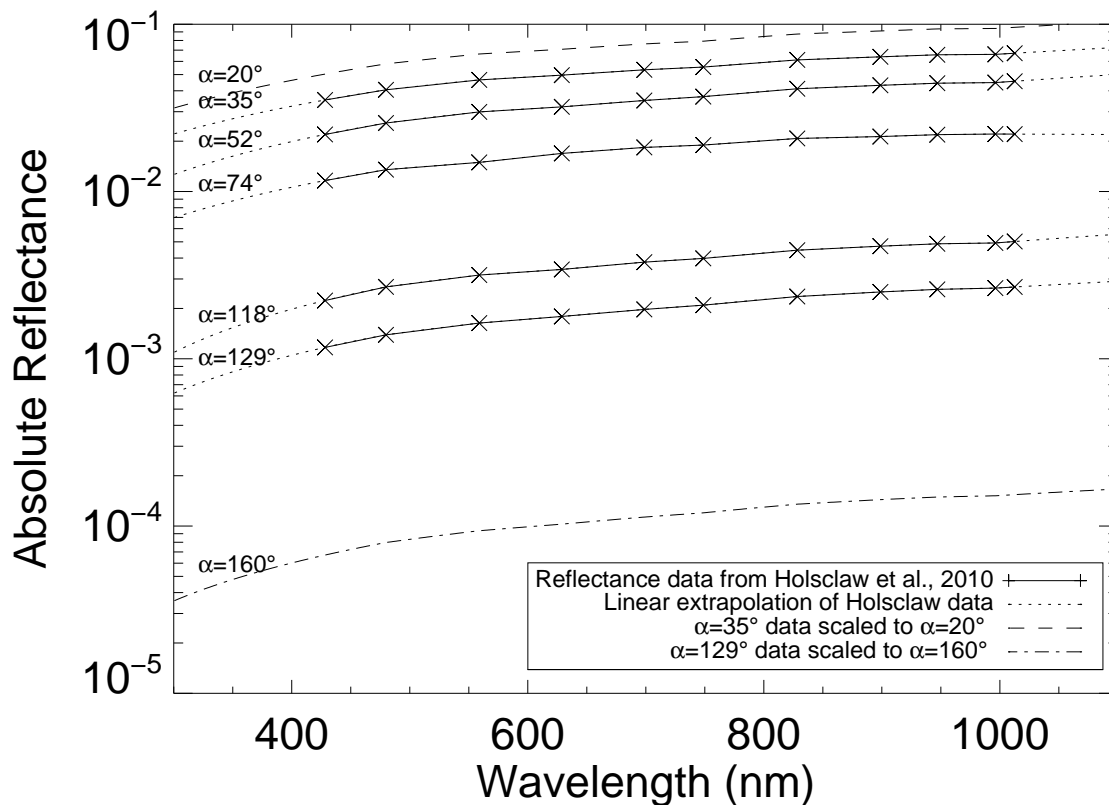


Fig. 3.— Absolute disk-integrated reflectance of Mercury at five phase angles, as measured by the MASCS and MDIS instruments on MESSENGER (Holsclaw et al. 2010). The MASCS/MDIS data have been linearly extrapolated to cover the full wavelength range over which the STEREO HI-1 instrument is sensitive. For synthetic Vulcanoids at phase angles outside the range (35° – 129°) covered by the observations, we scale the data by the V-band phase function of Mallama et al. (2002).

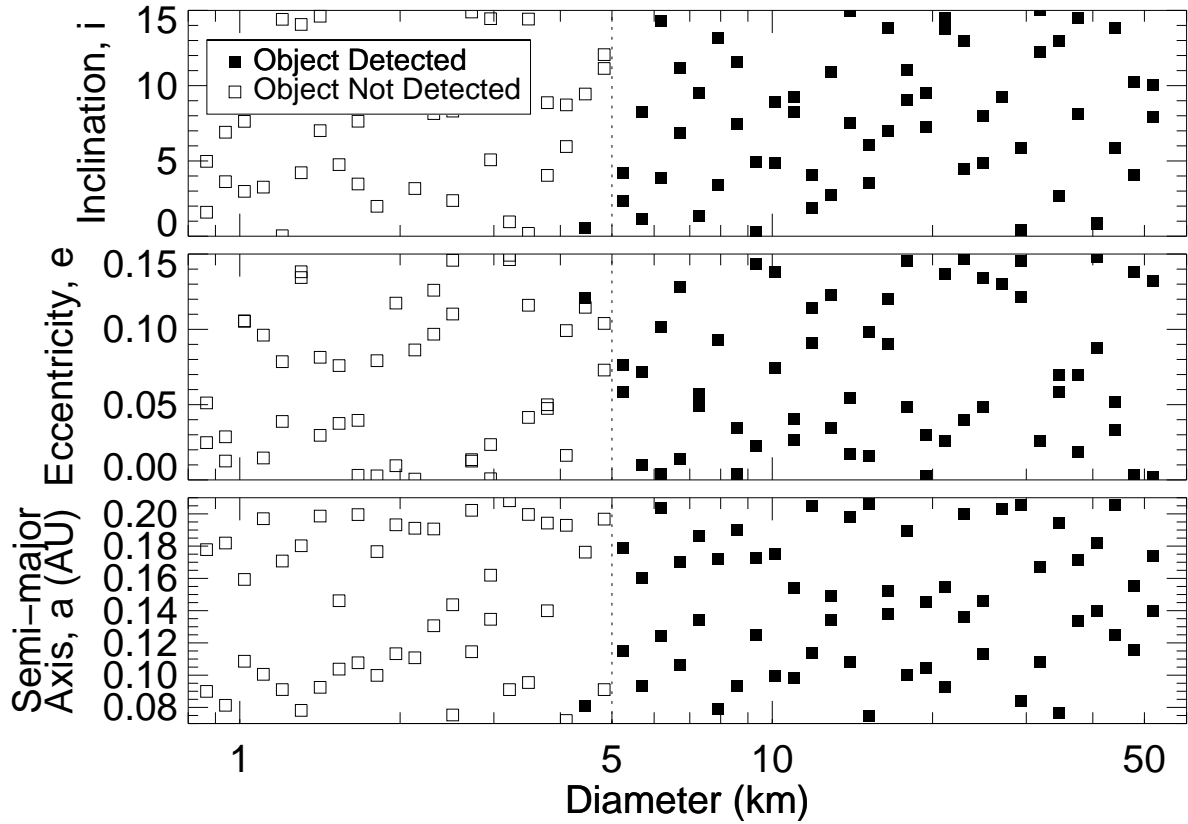


Fig. 4.— Orbital inclination, eccentricity and semi-major axis of synthetic Vulcanoids, as a function of the object’s diameter. Filled symbols represent Vulcanoids that were detected by at least one observer in our search, while open symbols were not detected by any of the four observers. There is no obvious correlation between a synthetic Vulcanoid’s orbital parameters (a , e , and i) and whether it was detected. In contrast, all objects larger than 5 km were detected, while only 1 object smaller than 5 km was detected.

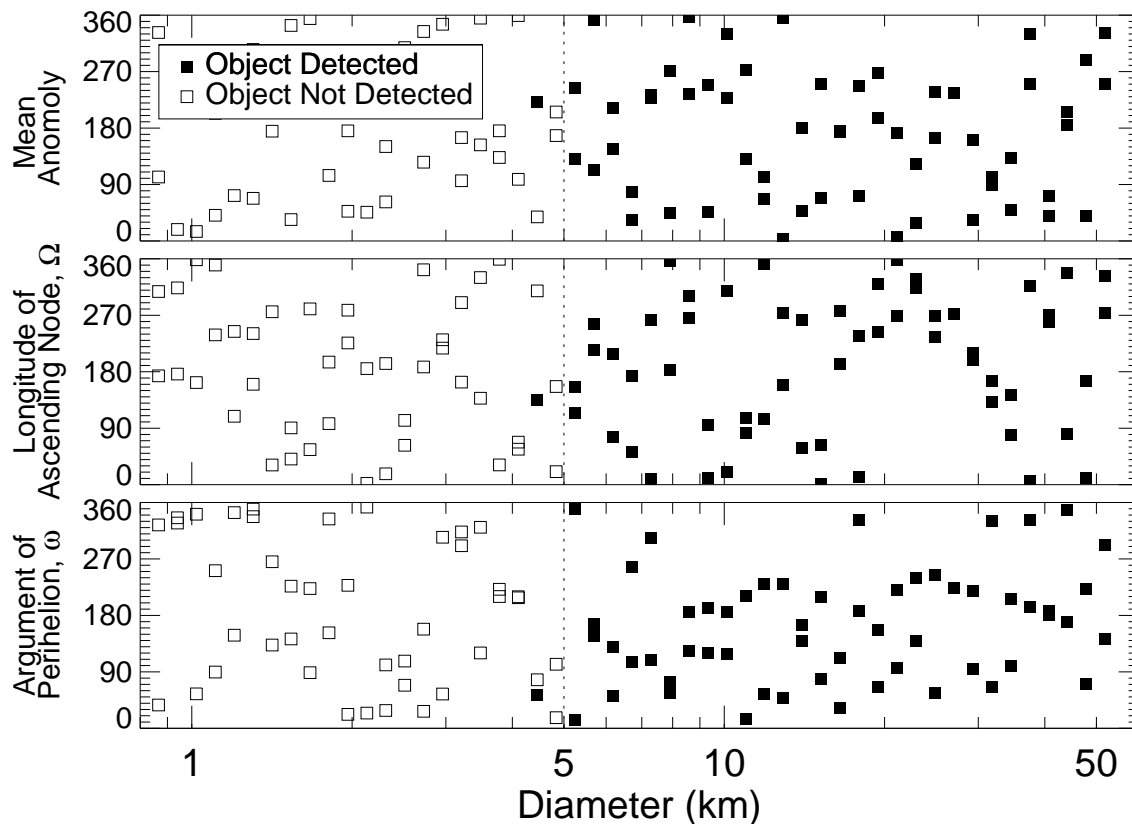


Fig. 5.— Mean anomaly, Longitude of the ascending node, and argument of perihelion of synthetic Vulcanoids, as a function of the object’s diameter. Filled symbols represent Vulcanoids that were detected by at least one observer in our search, while open symbols were not detected by any of the four observers. There is no obvious correlation between a synthetic Vulcanoid’s orbital parameters (ω , Ω , and M) and whether it was detected. In contrast, all objects larger than 5 km were detected, while only 1 object smaller than 5 km was detected.

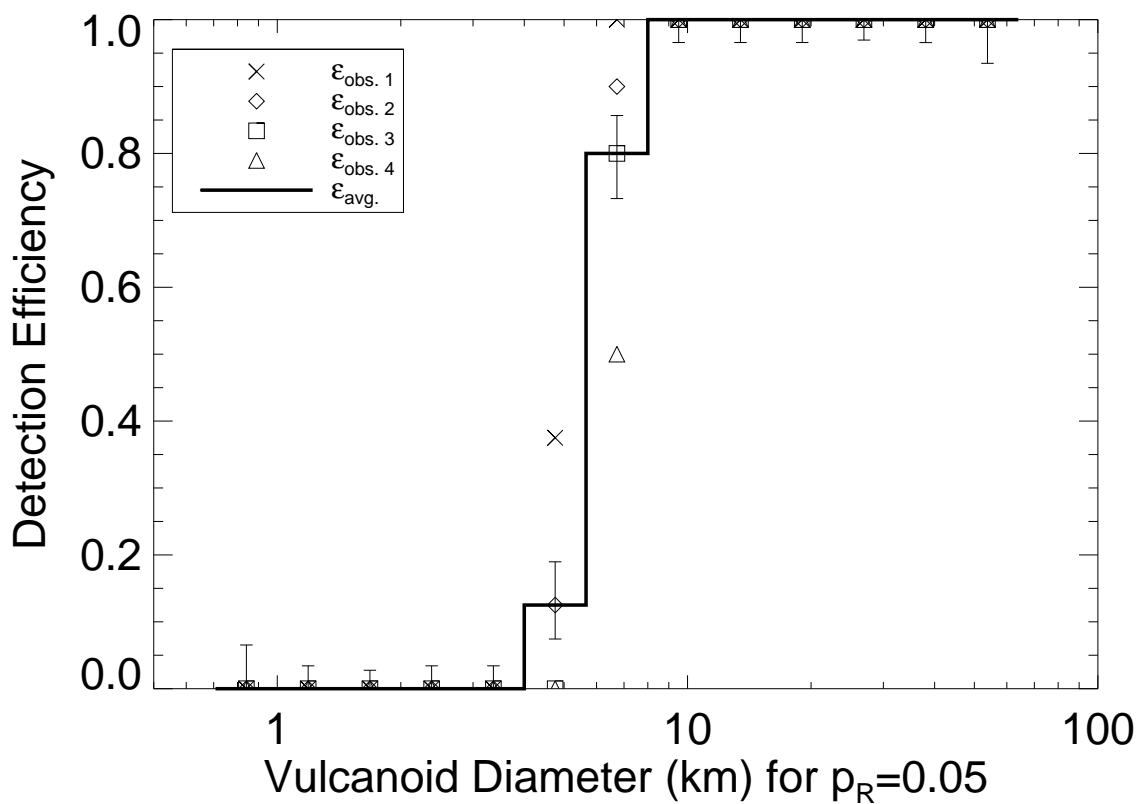


Fig. 6.— Efficiency of detecting synthetic Vulcanoids as a function of object diameter. The synthetic Vulcanoids are assumed to have an R-band albedo of 0.05 and a Mercury-like spectrum and phase function. For objects with a different assumed albedo, the diameter scales as $p_R^{-1/2}$. The observed detection efficiency for objects larger than 8 km is 1.0, while the observed detection efficiency for objects smaller than 4 km is 0.0. 1σ error bars are shown, based on the Monte Carlo analysis of the data in Table 1 described in the text. Given the average detection efficiency of 0.8 in the 5.7-8.0 km size bin, the probability of at least one observer detecting a real Vulcanoid of this size is 0.9984.